Appendix E—Evaluation of Magnitude-Scaling Relationships and Depth of Rupture

By Bruce E. Shaw[1]

Statement of the Problem

In the Uniform California Earthquake Rupture Forecast, version 2 (UCERF2) (Working Group on California Earthquake Probabilities, 2008), magnitude-area scaling relations were one of the main sources of uncertainty in the final hazard estimates. In this task, we seek ways of finding additional constraints or alternative methods of using scaling that will reduce these uncertainties.

Summary of Recommendations

A thorough study was made of the two main uses of magnitude-area relations: to calculate earthquake sizes, and to calculate earthquakes rates. A recently published paper (Shaw, 2013) discusses the issues and results more comprehensively than this study. Here, we summarize the recommendations for the Uniform California Earthquake Rupture Forecast, version 3 (UCERF3).

Earthquake Sizes

Continued use of magnitude-area scaling to estimate earthquake sizes is recommended. Area based on along-strike length and downdip width remains a good measure. Although questions have been raised concerning the depth extent of ruptures during large earthquakes, the seismogenic area remains a useful proxy for the purposes of estimating earthquake sizes.

Four relations are examined here in terms of their potential use. A fifth relation, the Somerville (2006) relation, was rejected based on its dependence on trimmed areas from inverse modeling, which introduces an intermediate step of highly nonunique, model, and smoothing-dependent processing of the data.

The four magnitude-area scaling relations examined for estimating earthquake sizes are (1) Ellsworth-B, (2) Hanks and Bakun (2002), (3) Shaw (2009), and (4) a Wells and Coppersmith-type linear relation between M and $\log_{10}A$. (1) The Ellsworth-B relation is:

$$M = \log A + 4.2 \tag{1}$$

It is extremely simple, a one-parameter fit, and a good empirical fit to the large earthquake (magnitude greater than 6.5 [M>6.5]) data it was developed to fit. (2) Hanks and Bakun (2002) is a two-regime scaling:

[1]Lamont-Doherty Earth Observatory, Columbia University.

$$M = \begin{cases} \log A + 3.98 & A \le 537 km^2; \\ \frac{4}{3}\log A + 3.07 & A > 537 km^2. \end{cases} \quad (2)$$

This scaling relation fits the data better at smaller magnitudes. (3) Shaw (2009) is a generalization of the Hanks and Bakun model; it extends the bilinear Hanks-Bakun two-regime scaling to a three-regime scaling that has a third asymptotic regime valid for very long ruptures (*L>>W)* whereby *S* approaches *W* scaling asymptotically. This is done at the expense of one additional scaling parameter (the length scale at which the transition to the third regime occurs). The Shaw (2009) scaling relation is parameterized as:

$$M = \log_{10} A + \frac{2}{3}\log_{10} \frac{\max(1, \sqrt{\frac{A}{W^2}})}{(1 + \max(1, \frac{A}{W^2 \beta}))/2} + const \ . \quad (3)$$

Here, *W* is the rupture width, and β is a fitting parameter that gives a crossover scale length to the asymptotic *W* scaling. To match the small earthquakes, the constant used is the same as in the Hanks-Bakun relation (*const*=3.98). In the limit of $\beta \to \infty$, the scaling relation reduces to the Hanks-Bakun scaling relation, and in this sense is a one-parameter extension of it, if *W* is treated as a parameter. In the limit as $L \to \infty$, it scales asymptotically as $M \sim \frac{2}{3}\log_{10} A$, which gives $S \sim W$, as the Starr (1928) and Knopoff (1958) solutions suggest. The means by which the parameters in this scaling relation are determined is discussed in Shaw (2013). For the UCERF3 fault model, β=7.4 is a suggested value, with $W=A/L$.

(4) The fourth magnitude-area scaling relation is a Wells and Coppersmith-type linear relation between *M* and $\log_{10} A$

$$M = C_1 \log_{10} A + C_0 \ . \quad (4)$$

The Ellsworth-B relationship is a special case of these linear relationships, with C_1=1. Here, the new parameter introduces a new scaling physics. Allowing for a nonspecific parameter on the area term, as the Wells-Coppersmith fitting does, adds substantial complexity to the model, given that it is an exponent on the area. Going from a discrete small set to a continuum is a leap in dimension; it must provide a much better fit to be worth generalizing in such a broad way.

Many databases were used to compare the scaling laws. Because of concerns about the potential influence of downdip width, the WGCEP03 database containing magnitude, length, and width was used (Working Group on California Earthquake Probabilities, 2003) to calibrate width-sensitive fits, in particular the Shaw09 (S09), equation (3) relation. The WGCEP03 database is mainly a subset of the Wells and Coppersmith (1994) data. The Hanks and Bakun (2008) magnitude-area database was used as another target, providing additional large earthquakes and alternative interpretations of areas, particularly at small magnitudes. Finally, supplemental data compiled by Biasi and others (appendix F, this report) as part of the UCERF3 effort was used as a test of how well the scaling relations fit newer datasets that they were not optimized against.

Figure E1 shows plots of the data and scaling relations fit to the data. Standard deviations of fits relative to the data are shown in table E1, with the models listed in rank order based on

Akaike information criterion (AIC) (Akaike, 1974). With AIC, minimizing of errors is rewarded and extra parameters are penalized; minimum AIC is best. $AIC = -2 \ln \mathcal{L} + 2k$, where $\mathcal{L}$ is the likelihood and k is the number of fitted parameters. Therefore, differences in AIC correspond to differences in log-likelihood, with the relative likelihood of two models represented as $e^{-\Delta AIC/2}$. This gives a scale of the differences in AIC that matter–at least a few to be significant. AIC is similar to the Fisher F-Test in that they both examine the importance in the fit relative to the cost of extra parameters. AIC has an advantage in that it does not require the lower-parameter model to be embedded in the higher-parameter model. Used together, standard deviation and AIC provide a helpful view of differences in fits. Differences in standard deviation give relative differences in how well the curves are fitting in an absolute sense, while differences in AIC give a sense of how statistically significant, in a log-likelihood sense, the differences are.

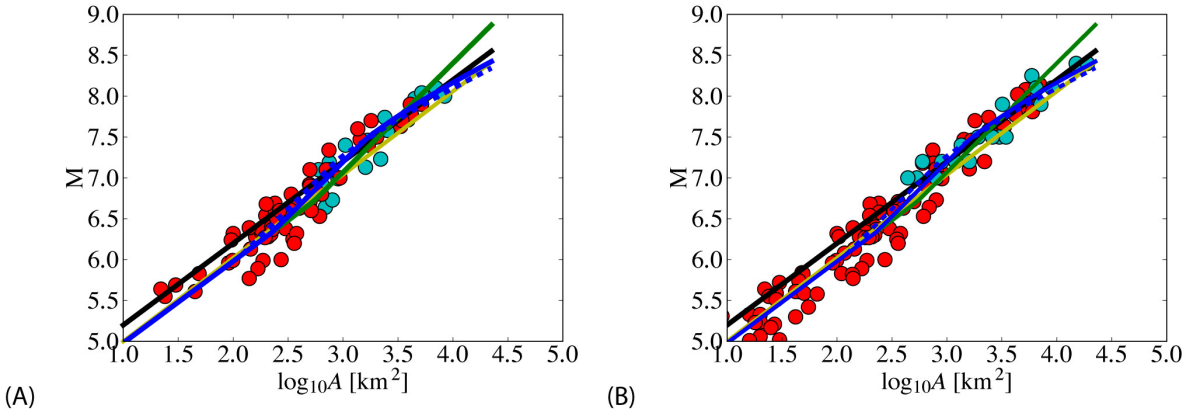

Figure E1. Graphs showing magnitude area relations for large strike-slip earthquakes. *A*, WGCEP03 data. Red circles denote W<15 km events, cyan circle denote *W*>15 km events. *B*, Red circles denote magnitude and area of events from Hanks and Bakun (2008) database. Cyan circles are from Biasi and others (appendix F, this resport) database. Curves are fit to Hanks and Bakun (2008) database, with appendix F data shown for comparison. Black line is linear Ellsworth-B (Working Group on California Earthquake Probabilities, 2003) magnitude-area relation, equation 1. Green line is Hanks and Bakun (2002) bilinear relation, equation 2. Yellow line is Wells and Coppersmith (1994) scaling relation, equation 4. Blue line is Shaw (2009) scaling relation, equation (3). The S09′ relation is shown using default *W* values; solid blue line is *W*=15 km, and dashed blue line is *W*=11 km.

One issue concerning fits to the data is whether fits across the entire earthquake magnitude range, or only fits at the large earthquakes, should be considered, given that the small earthquakes may be especially uncertain but yet they are also used in hazard calculations. Both sets of error measures, therefore, are shown in table E1.

Fits to the WGCEP03 data are shown in table E1a . Fits are restricted to $M > 6.5$ earthquakes in table E1b. The Hanks-Bakun data are shown in table 1c, and fits to $M > 6.5$ earthquakes for that data are shown in table E1d. Because only area values are given in the Hanks-Bakun database, the Shaw09 relation fixes W as a parameter in fitting that data. Fits to the earthquakes added by Biasi and others (appendix F, this report) are shown in table E1e. These data show the accuracy of model scalings with respect to earthquakes on which they were not regressed.

Table E1. Magnitude-area scaling fits.

[The standard deviation ("Std. dev.") measures the difference in magnitudes of the data from the predicted curve. A least squares fit is done, which disregards errors in area relative to errors in magnitude. The number of free parameters is given by "No.," with the best fitted parameter values following that. The parameter C_0 is the constant in the magnitude-area scaling relations. Other parameters are defined at the individual equation numbers ("Eqn"). Ranking in this table, and those that follow, is by minimum AIC (Akaike, 1974), in which standard deviation is rewarded but additional parameters are penalized. $AIC = -2 \ln \mathcal{L} + 2k$, where $\mathcal{L}$ is the likelihood and k is the number of fitted parameters. Here $AIC = n(\ln(2\pi\sigma^2) + 1) + 2k$, where σ is the standard deviation, n is the number of data points, and k is the number of parameters. (a) Data from the WGCEP03 database (Working Group on California Earthquake Probabilities, 2003). The modified Wells-Coopersmith scaling is denoted with a dagger symbol: WC†. The S09 scaling with fixed values of W is denoted with a prime symbol: S09′. (b) Only large-magnitude earthquakes (magnitude greater than 6.5 [$M>6.5$]) are considered, reducing the number of data points from 77 to 49. Because the parameters are not refit to the reduced data set, we mark the AIC with a star, AIC*, to indicate that the parameter penalties perhaps are overly harsh, because the parameters are not refit. However, the AIC values help as to the statistical significance of the differences in the standard deviations, so they are still presented. This approach favors the Ellsworth-B scaling because it was designed to fit across this range, while the other scalings were fit across the entire range. (c) Data from the Hanks-Bakun database (Hanks and Bakun, 2008). Because width information is unavailable, only S09′ fixed W solutions are shown. Two of those are shown: one optimized for the Hanks-Bakun data, and the other a default version based on the WGCEP03 data. (d) Only large magnitude earthquakes ($M>6.5$) are considered, reducing the number of data points from 87 to 36. This favors the Ellsworth-B scaling. (e) Misfits to new events in the Biasi and others (appendix F, this report) database. Formal uncertainties in the parameter fits are at the 10-percent level.]

(a) Fits to complete WGCEP03 magnitude-area-width dataset.

Scaling		Best fits		Parameters			
Name	Eqn	Std. dev.	AIC	No.	Best fit values		
S09	(3)	.202	-23.62	2	$C_0 = 3.98$	$\beta = 7.4$	
WC†	(4)	.203	-22.87	2	$C_0 = 3.89$	$C_1 = 1.08$	
S09′	(3)	.204	-20.65	3	$C_0 = 3.98$	$\beta = 7.4$	$W = 15$ km
HB	(2)	.212	-16.13	2	$C_0 = 3.98$	$A_C = 537$ km^2	
WC	(4)	.217	-12.50	2	$C_0 = 3.98$	$C_1 = 1.02$	
EB	(1)	.229	-6.15	1	$C_0 = 4.20$		

(b) Misfits to magnitude greater than 6.5 subset of WGCEP03 data without refitting parameters.

Scaling		Misfits $M > 6.5$		Parameters			
Name	Eqn	Std. dev.	AIC*	No.	Values		
EB	(1)	.173	-31.09	1	$C_0 = 4.20$		
S09	(3)	.177	-26.23	2	$C_0 = 3.98$	$\beta = 7.4$	
WC†	(4)	.178	-26.32	2	$C_0 = 3.89$	$C_1 = 1.08$	
S09′	(3)	.190	-17.60	3	$C_0 = 3.98$	$\beta = 7.4$	$W = 15$ km
HB	(2)	.213	-8.72	2	$C_0 = 3.98$	$A_C = 537$ km^2	
WC	(4)	.216	-7.17	2	$C_0 = 3.98$	$C_1 = 1.02$	

(c) Fits to complete Hanks-Bakun magnitude-area dataset.

Scaling		Best fits		Parameters			
Name	Eqn	Std. dev.	AIC	No.	Best fit values		
S09′	(3)	.208	-20.54	3	$C_0 = 3.98$	$\beta = 5.0$	$W = 19$ km
HB	(2)	.213	-18.46	2	$C_0 = 3.98$	$A_C = 537$ km^2	
WC†	(4)	.215	-16.43	2	$C_0 = 3.86$	$C_1 = 1.08$	
S09′	(3)	.213	-17.58	3	$C_0 = 3.98$	$\beta = 7.4$	$W = 15$ km
WC	(4)	.220	-12.32	2	$C_0 = 3.98$	$C_1 = 1.02$	
EB	(1)	.275	24.23	1	$C_0 = 4.20$		

Table E1.—continued

(d) Misfits to magnitude greater than 6.5 subset of Hanks-Bakun data without refitting parameters.

Scaling		Misfits $M > 6.5$		Parameters			
Name	Eqn	Std. dev.	AIC*	No.	Values		
EB	(1)	.185	-17.26	1	$C_0 = 4.20$		
WC†	(4)	.193	-12.21	2	$C_0 = 3.86$	$C_1 = 1.08$	
S09′	(3)	.200	-7.58	3	$C_0 = 3.98$	$\beta = 5.0$	$W = 19$ km
S09′	(3)	.204	-6.32	3	$C_0 = 3.98$	$\beta = 7.4$	$W = 15$ km
HB	(2)	.213	-5.27	2	$C_0 = 3.98$	$A_C = 537$ km^2	
WC	(4)	.216	-4.05	2	$C_0 = 3.98$	$C_1 = 1.02$	

(e) Misfits to Biasi and others (appendix F, this report) magnitude-area-width data without refitting parameters.

Scaling		Best fits		Parameters		
Name	Eqn	Std. dev.	AIC*	No.	Best fit values	
EB	(1)	.145	-17.34	1	$C_0 = 4.20$	
S09	(3)	.165	-10.65	2	$C_0 = 3.98$	$\beta = 7.4$
WC†	(4)	.175	-8.24	2	$C_0 = 3.86$	$C_1 = 1.08$
WC	(4)	.210	-1.27	2	$C_0 = 3.98$	$C_1 = 1.02$
HB	(2)	.234	2.69	2	$C_0 = 3.98$	$A_C = 537$ km^2

The Hanks-Bakun and S09 relations work best across the entire earthquake magnitude range, while Ellsworth-B and S09 relations work best for large earthquakes. The original Wells-Coppersmith relation (WC in the table) underpredicts the Hanks-Bakun dataset at large earthquakes. Refitting the parameters, we find best fitting C_1=1.08 and C_0=3.86 (WC† in the table), which is more accurate than the original relation. However, the nonrobustness of the fits (in particular changing C_1 for other different datasets) raises issues for this functional form. When information about width is available, the Shaw09 relation works better with fault-based W (shown as S09 in the tables) than fixed values of W (shown as S09′ in the tables), so this is the preferred version of that relation.

Comparing fits of the different scaling laws, in log-log magnitude-log area space, across the entire range of earthquake magnitudes (M>5), the Shaw09, Hanks-Bakun, and Modified Wells-Coppersmith type scalings fit better than the Ellsworth-B scaling. For only the large earthquakes (M>6.5), however, which the Ellsworth-B relation was developed to match, it does well. Using as an error metric the difference in magnitude, Fisher F-tests support what we see in AIC: from the lowest magnitudes (M>5), the S09 relation fits better than the Ellsworth-B relation, as does the Hanks-Bakun relation relative to the Ellsworth-B relation. For large-magnitude earthquakes (M>6.5), the Ellsworth-B relation begins to fit better. At large earthquake magnitudes, the Ellsworth-B, S09, and Modified Wells-Coopersmith relations are comparable. In contrast, the Hanks-Bakun relation begins to do less well at large earthquake magnitudes. For the entire magnitude range, the S09 relation fits better than the Hanks-Bakun relation, significantly in the WGCEP03 data where width information is available, though only just above the level of statistical significance in the Hanks-Bakun data where width data is unavailable and default W values must be used. As the magnitude cutoff increases, the S09 relation does even better compared to the Hanks-Bakun relation. Therefore, the extra regime in S09 relative to Hanks-Bakun appears justified in terms of a statistically better fit. In fitting the new Biasi and others (appendix F, this report) data, the Ellsworth-B relation does the best job.

Weighting Recommendation for Earthquake Sizes

With respect to weighting, one possibility would be to weight equally all relations within an acceptable AIC difference. Other weightings can also be justified by data uncertainties or theoretical constraints (for example, a desire for more consistency between scalings used for sizes and rates).

The original values for Wells-Coppersmith-type relations do not fit well enough at large earthquake magnitudes to justify their use. The modified values could be used as a fit to the data. However, nonrobustness of parameter fits and difficulty connecting to other data fits, are arguments against using modified values.

Rate of Events

In UCERF2, rates of earthquakes were calculated by moment balancing, with all of the moment from the magnitude-area scaling assumed to occur spread evenly with depth over the seismogenic rupture area. This leads to two major sources of uncertainty. One is the differences in the scaling laws, which have different estimated slips for a given area at very large earthquakes that dominate the sums in the moment balancing. A second source of uncertainty is the question of whether the slip might extend deeper below the seismogenic layer during large earthquakes, a question raised by efforts to reproduce scaling laws (Das, 1982; King and Wesnousky, 2007) by dynamic models (Shaw and Wesnousky, 2008) and by kinematic ground motion modeling efforts (Graves and others, 2011). We propose to address this issue by treating the balancing in terms of slip rate, and expanding the data considered to include geologically observable surface slip data. Slip rate would be targeted to balance at mid-seismogenic depths.

An extensive study of surface slip data and slip-length scaling laws has been done and shown to be a viable pathway for inclusion in the slip rate balancing estimates (Shaw, 2013). Qualitative consistency with estimates from magnitude-area scaling was seen, but systematic quantitative differences of 30 percent were seen in slip estimated from surface-slip measurements, relative to slip estimated from magnitude assuming all the moment occurs over the seismogenic area. Two end-member cases are possible. One end member would have the surface-slip estimates biased low, with missing slip occurring below measurement detection, perhaps through plastic deformation in unconsolidated sediments. The second end member would have the magnitude-area estimates biased high, with deeper subseismogenic slip mapped onto seismogenic depths. Both end members remain possibilities, as does some compromise mixture of a value between the end members involving some of both these possible biasing effects. We therefore recommend representing both types of estimates in the logic tree.

Implied Slip-Length from Magnitude-Area

Magnitude-area scaling can be transformed into a corresponding implied slip-length scaling (Shaw, 2013). In the moment balancing or slip-rate balancing use of the magnitude-area scaling relations, the slip from each earthquake is summed to get an overall rate of earthquakes to match the long-term slip rate on the faults. Because this slip is summed linearly, it makes sense to see how the scaling laws look not in log-log space, which emphasizes the range of sizes, but in linear-linear space, which emphasizes the largest earthquakes that are dominating the sum. To convert the magnitude-area scaling laws to implied slip-length scaling laws, we use the same assumptions involved in moment balancing. We convert magnitude M to moment $\mathcal{M}$ and divide by area A and modulus μ to get slip S: $S=\mathcal{M}/A\mu$. A standard value of the modulus is used (μ=30

gigapascals [GPa]). Here, we see the uncertainty in the downdip width: if our area estimates are biased, our slip estimates will be biased. For length and width, we can use the information in databases directly when it is available, as in the WGCEP03 data. This transformed data is shown in figure E2*A*. When it is unavailable, as in the Hanks-Bakun data, we can divide the area by downdip width W to get length L: $L=A/W$. This transformation is shown in figure E2*A* assuming W equals L for small earthquakes, but then saturates for large earthquakes at the downdip width W . That is, $W=W^*$ where

$$W^* = \min(L,W) = \begin{cases} L & L \le W; \\ W & L > W \end{cases} \tag{5}$$

with typical values of the seismogenic width W=15 kilometers (km) for vertical strike-slip faults, and downdip widths for dipping faults having correspondingly larger values. Assuming a default downdip width, as in equation 5, we can infer an L from A. Alternatively, individual values of L from compiled databases (for example, Wells and Coppersmith [1994]) can be used directly with the Hanks-Bakun data. We also have determined that when we use individual values of L associated with earthquakes; we get similar results whether we assume a default value for W and derive an implied L or use individual values of L. Although individual points move, the overall trend is similar. Because of the simplicity and clarity associated with using implied length in conjunction with implied slip, we focus our attention on that approach when using the Hanks-Bakun data here.

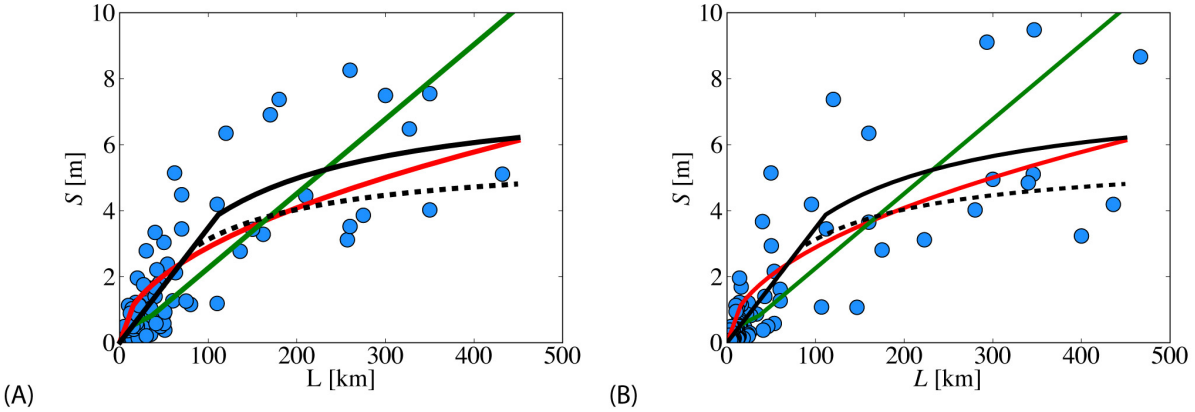

Figure E2. Graphs showing fits of implied slip-length scaling by magnitude-area scalings. (*A*) Data are derived from WGCEP03 database. Earthquake-specific Ws are used. (*B*) Data are derived from Hanks-Bakun database. Default W=15 km. Magnitude is converted to moment, then divided by area and modulus to calculate slip. When length is available in database, it is used. Otherwise, area is converted to length by dividing area by width assuming seismogenic depth H=15 km. Data are shown with light blue circles. Different color lines represent different magnitude-area scaling laws rescaled the same way in which the data have been rescaled. Parameters are used directly from magnitude-area scaling laws, table E2a. The curves are the implied slip-length for Ellsworth-B (Working Group on California Earthquake Probabilities, 2003) (red), Hanks-Bakun (Hanks and Bakun, 2008) (green), and Shaw (2009) (black). The S09′ relation is shown using default W values; solid black line is W=15 km, dashed black line is W=11 km.

Assuming again that $W=W^*$, the magnitude-area scaling laws transform into slip-length scaling laws as follows. For Ellsworth-B, we get

$$S \sim A^{1/2} = C_2 (LW^*)^{1/2} = \begin{cases} C_2 L & L \le W; \\ C_2 (LW)^{1/2} & L > W \end{cases} \tag{6}$$

For generalized Wells-Coppersmith type scaling, we get

$$S \sim A^{1.5C_1-1} = C_3 (LW^*)^{1.5C_1-1} = \begin{cases} C_3 L^{3C_1-2} & L \le W; \\ C_3 (LW)^{1.5C_1-1} & L > W \end{cases} \tag{7}$$

For Hanks-Bakun, we get

$$S \sim \begin{cases} (\frac{A}{537})^{1/2} & A \le 537 km^2; \\ \frac{A}{537} & A > 537 km^2 \end{cases} = \begin{cases} C_4 L & L \le W; \\ C_4 (LW)^{1/2} & W < L < 537 km^2 / W \\ C_4 LW / (537)^{1/2} & 537 km^2 / W \le L \end{cases} \tag{8}$$

For Shaw09, we get

$$S \sim \frac{2A/W}{1+\max(1, A/W^2\beta)} = \begin{cases} C_5 L & L \le W\beta; \\ \frac{2C_5}{\frac{1}{L}+\frac{1}{W\beta}} & L > W\beta \end{cases} \tag{9}$$

Taking into account the crossover effects of the finite seismogenic width expressed in equation 5, the magnitude-area scaling laws transformed into slip-length scaling laws are modified to have an additional scaling regime for the Ellsworth-B and Hanks-Bakun scaling, while the Shaw09 scaling is reduced by one regime and one parameter, from three to two regimes, and from three to two parameters (C_5 and $W\beta$ in equation [9]). This reduction for the Shaw09 scaling is not coincidental because it was developed from a slip-length scaling law.

Comparing the different scalings for large L, we note very different predicted behaviors. For $L>>W$: in Hanks-Bakun, $S \sim L$; in Ellsworth-B, $S \sim L^{1/2}$; and in Shaw09, $S \sim W$. In the generalized Wells-Coopersmith scaling, $S \sim L^{1.5C_1-1}$, a nonspecific exponent. The scalings also differ in their W dependence at large L, with a linear dependence on W in Hanks-Bakun and Shaw09, and a $W^{1/2}$ dependence in Ellsworth-B. In the generalized Wells-Coopersmith scaling, $S \sim W^{1.5C_1-1}$, again a nonspecific exponent . Unfortunately, the W values for the data are too uncertain to test the different predicted dependences. Fortunately, the data appear sufficient to test some features of the L dependence.

Table E2. Implied slip-length from magnitude-area.

The standard deviation ("Std. dev.") in table E2 measures the difference in slip of the data from the predicted curve. The data are transformed from magnitude-area to slip. We do not refit the parameters, which were set based on fits in log space magnitude-log area, to the new linear space slip-length metric. When we do not refit the parameters, with denote this with AIC*. (a) Transformed data from WGCEP03 data (Working Group on California Earthquake Probabilities, 2003). Lengths from database. (b) Transformed data from Hanks-Bakun database (Hanks and Bakun, 2008). Lengths from dividing area by default width, with seismogenic width of 15 kilometers. (c) Surface slip-length scaling relations are fit to the implied slip-length Hanks-Bakun data. This is done for completeness, and for comparison with the surface slip-length data. Formal uncertainties in parameter fits are at the 10-percent level in tables E2a–c.

(a) Misfits without rescaling for new metric; from WGCEP03 data.

Scaling		Unrescaled Misfit		Parameters		
Name	Eqn	Std. dev.	AIC*	No.	Values	
S09	(3)	1.212	252.1	2	$C_0 = 3.98$	$\beta = 7.4$
S09′	(3)	1.245	256.3	2	$C_0 = 3.98$	$W\beta = 15 * 7.4 = 111$ km
EB	(1)	1.275	258.0	1	$C_0 = 4.20$	
WC†	(4)	1.415	276.0	2	$C_0 = 3.86$	$C_1 = 1.08$
HB	(2)	1.687	303.0	2	$C_0 = 3.98$	$A_C = 537$ km^2
WC	(4)	1.699	304.1	2	$C_0 = 3.98$	$C_1 = 1.02$

(b) Misfits without rescaling for new metric; from Hanks and Bakun (2008) data.

Scaling		Unrescaled Misfit		Parameters		
Name	Eqn	Std. dev.	AIC*	No.	Values	
S09′	(3)	1.180	279.6	2	$C_0 = 3.98$	$W\beta = 15 * 7.4 = 111$ km
EB	(1)	1.211	282.2	1	$C_0 = 4.20$	
WC†	(4)	1.282	294.1	2	$C_0 = 3.86$	$C_1 = 1.08$
HB	(2)	1.459	316.6	2	$C_0 = 3.98$	$A_C = 537$ km^2
WC	(4)	1.549	327.0	2	$C_0 = 3.98$	$C_1 = 1.02$

(c) Surface slip scaling relations fit to Hanks-Bakun implied slip-length data.

Scaling		Best fits		Parameters		
Name	Eqn	Std. dev.	AIC	No.	Best fit values	
L^{η}	(12)	1.190	281.1	2	$C_8 = 0.026$	$\eta = .632$
$L^{1/2}$	(10)	1.236	285.8	1	$C_6 = 7.46 \cdot 10^{-5}$	
S12	(13)	1.249	287.6	1	$\Delta\sigma = 5.95$ MPa	
L	(11)	1.339	299.7	1	$C_7 = 1.19 \cdot 10^{-6}$ / km	

Looking at the fits of the transformed scaling laws to the transformed data in table E2, the Shaw09 relation is the best, followed closely by Ellsworth-B, and then the Modified Wells-Coopersmith and Hanks-Bakun.

Surface Slip Data

The use of surface slip data to constrain rates has a number of advantages. First, it avoids some of the uncertainty around the issue of the depth of rupture in large earthquakes. Second, it adds to the analysis a new, independent, geologically observable dataset, thereby adding testable and collectible information to the estimates. Third, by using slip (which is a linear measure) rather than magnitude (which is a logarithmic measure) as the independent variable, fits to the scaling laws are more naturally mapped onto the linearly summed integral constraints, so errors are better accounted for where they matter most. Finally, the use of surface slip data enables incorporation of pre-instrumental information, making possible much extended datasets.

A more thorough study has been done using this approach, and has been recently published (Shaw, 2013). Four candidate scalings emerged. The first scaling is a square root $L^{1/2}$ scaling consistent with the implied Ellsworth-B scaling:

$$S \sim A^{1/2} = C_6 (LW)^{1/2} \tag{10}$$

This kind of scaling has been proposed by Leonard (2010) for large lengths. The second scaling is a linear L scaling consistent with the implied Hanks-Bakun scaling for the largest earthquakes:

$$S \sim A = C_4 LW \tag{11}$$

The third scaling is a power law scaling, consistent with the generalized Wells-Coppersmith type scaling. This adds an extra free parameter, a nonspecific exponent η, in the scaling, so a much better fit will be needed to make the added model complexity and potential physics worthwhile:

$$S \sim A^{\eta} = C_8 (LW)^{\eta} \tag{12}$$

The fourth scaling is a constant stress drop scaling:

$$S = \frac{\Delta\sigma}{\mu} \frac{1}{\frac{7}{3L} + \frac{1}{2W}} \tag{13}$$

with μ the shear modulus and $\Delta\sigma$ the stress drop. This relationship comes from a more careful treatment of how slip would be expected to transition from circular ruptures beginning to break the surface to long rectangular ruptures. A generalization of the constant stress drop model for dipping faults and oblique slip is detailed in section on "Dipping Faults" below.

The scalings fit to the UCERF3 data compiled by Biasi and others (appendix F, this report) are shown in figure E3. Fits of the scalings to the data are shown in table E3. Fits to the data from appendix F are shown in table E3a. Fits to the California-only data from appendix F are shown in table E3b. Fits to an older data set compiled by Wesnousky (2008) are shown in table E3c. Comparing the fits, the amplitudes fitting scaling relations to California-only data are about 5–10 percent smaller than amplitudes found fitting the full new appendix F data. Comparing the old Wesnousky (2008) data to the new Biasi and others (appendix F, this report) data, the amplitudes from fitting increase about 15 percent, and the standard deviations increase about 40 percent, but the overall conclusions remain similar. In both cases, the forms trending towards sublinear scaling, where slip increases less and less as earthquakes get longer, substantially outperform the linear scaling model. This is consistent with previous work noting the breakdown in the "L" model scaling for very large aspect ratio earthquake (Romanowicz, 1992; Scholz, 1994).

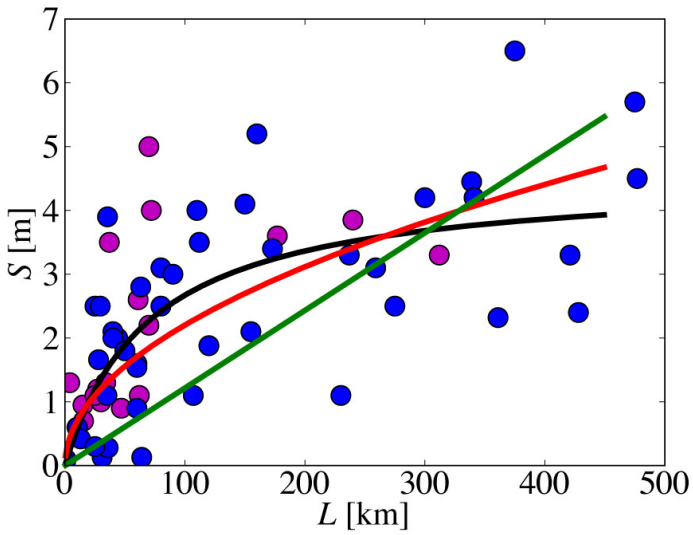

Figure E3. Graph showing fits of surface slip-length scaling laws to surface slip observations of average slip versus length using Biasi and others (appendix F, this report) database. Color indicates focal mechanism: strike-slip shown in blue, dip-slip in magenta. Curves only fit to strike-slip data. In order of best fit to least-good fit: black line shows equation 13, constant stress drop scaling; red line shows equation 10, $L^{1/2}$ scaling; and green line shows equation 11, L scaling. Note the change in vertical axis scale in figure E2 compared to figure E3, showing the overall systematic difference, and fundamental epistemic uncertainty, in average slip estimates from magnitude-area versus surface slip observations. Some of this difference represents different earthquakes in the two different databases, but some of it, a difference of about 30 percent, remains when we restrict our view to the same earthquakes. Note also the overall qualitative consistency in trends of the two types of data in both figures.

Table E3. Slip length from surface slip data.

[The standard deviation ("Std. dev.") measures the difference in slip of the data from the predicted curve. The table shows a comparison of the surface slip data with scaling relations proposed for surface slip-length scaling. (a) Fits to Biasi and others (appendix F, this report) data. There are 45 data points in the fit to the strike-slip data. The best overall fit to the data, in terms of AIC, is S12, the constant stress drop model, equation 13, followed closely by the $L^{1/2}$ model, equation 10. (b) Fits to Biasi and others (appendix F, this report) California-only data. In this case, there are only 16 data points. Excluding the power law fit, the best fitting parameters change only slightly—about 5–10 percent—less in amplitude than the full dataset. The top models remain close, but swap places slightly. The scatter is also reduced in this restricted dataset. (c) Fits to the older (Wesnousky, 2008) data. Excluding the power law fit, the main change for the new fits relative to the old fits are that the amplitude of the fits increases about 15 percent with the new data, and the scatter, reflected in the standard deviation, increases about 40 percent. With respect to the power law fits across the different datasets, note the parameter sensitivity of η to the datasets. This is an undesirable quality of a measure, and argues against the extension of dimension in this direction. In contrast, the covariance of the fits $L^{1/2}$, S12, and L to the different datasets is substantial; they are varying stably together]

(a) Fits to Biasi and others (appendix F, this report) data.

Scaling		Best fits		Parameters		
Name	Eqn	Std. dev.	AIC	No.	Best fit values	
S12	(13)	1.12	139.6	1	$\Delta\sigma = 4.54$ MPa	
L^{η}	(12)	1.11	141.4	2	$C_8 = 0.142$	$\eta = .387$
$L^{1/2}$	(10)	1.14	141.5	1	$C_6 = 5.69 \cdot 10^{-5}$	
L	(11)	1.52	167.1	1	$C_7 = 8.10 \cdot 10^{-7}$ / km	

Table E3.—continued

(b) Fits to Biasi and others (appendix F, this report) California-only data.

Scaling		Best fits		Parameters		
Name	Eqn	Std. dev.	AIC	No.	Best fit values	
S12	(13)	.659	34.0	1	$\Delta\sigma = 4.14$ MPa	
$L^{1/2}$	(10)	.666	34.4	1	$C_6 = 5.33 \cdot 10^{-5}$	
L^{η}	(12)	.664	36.3	2	$C_8 = 0.066$	$\eta = .474$
L	(11)	1.08	49.8	1	$C_7 = 8.02 \cdot 10^{-7}$ / km	

(c) Surface slip scaling relations using adapted older (Wesnousky, 2008) data.

Scaling		Best fits		Parameters		
Name	Eqn	Std. dev.	AIC	No.	Best fit values	
S12	(13)	.760	50.05	1	$\Delta\sigma = 3.91$ MPa	
$L^{1/2}$	(10)	.804	52.43	1	$C_6 = 4.91 \cdot 10^{-5}$	
L^{η}	(12)	.788	53.60	2	$C_8 = 0.093$	$\eta = .421$
L	(11)	1.174	68.34	1	$C_7 = 7.10 \cdot 10^{-7}$ / km	

Note in table E3 that the exponent on the power law scaling (equation 12) is not very stable with change of dataset, unlike amplitudes of other fits, which covary. The sensitivity of this parameter makes it much less useful as a fitting parameter. This also argues against generalizing to that continuum parameter.

Sublinear Scaling

Both the implied slip versus length and the surface slip versus length curves show sublinear scaling. The data very clearly support sublinear scaling—that is, increases in slip with length that increase at smaller rates as the lengths get larger. Sublinear scaling is shown in figure E4. Cumulative slip versus cumulative length, for the data points rank ordered in length, is shown in figure E4*A*. The downward curvature indicates the sublinear scaling. In contrast, linear scaling would imply a constant slope, while upward curvature would imply supralinear scaling. This cumulative curve gives a robust qualitative picture. However, the details of the form depend on the density of points along the length axis, so more quantitative measures need a different approach. Local average slopes in the data are shown in figure E4*B*. Average slope given by average slip divided by average length, versus length, are plotted there. The averages are calculated across neighboring data points, averaged across $n = 3, 4, 5$ data points, represented by different color symbols, in the plot. For the implied slip, in Figure E4*B* we see, at long length scales of 100 km and more, a systematic decrease in the slope with increasing length. In the plot, we also show with solid lines the implied slopes from magnitude-area curves. We see a good fit for Ellsworth-B and S09, a poor fit functionally for Hanks-Bakun, and an underfit for Wells-Coopersmith to the implied slope from the Hanks and Bakun (2008) data.

The sublinear trend is even more evident in the average slope of the surface slip-length data. The same type of plot as in Figure E4*B* is also shown in figure E4*D*, now using surface slip data (appendix F, this report). The plots also show in solid lines the slopes for the different scaling laws. The $L^{1/2}$ and the constant stress drop models both work well. The constant-slope linear fit again is a very poor functional fit. We do not show the power-law fit owing to sensitivities in the exponents.

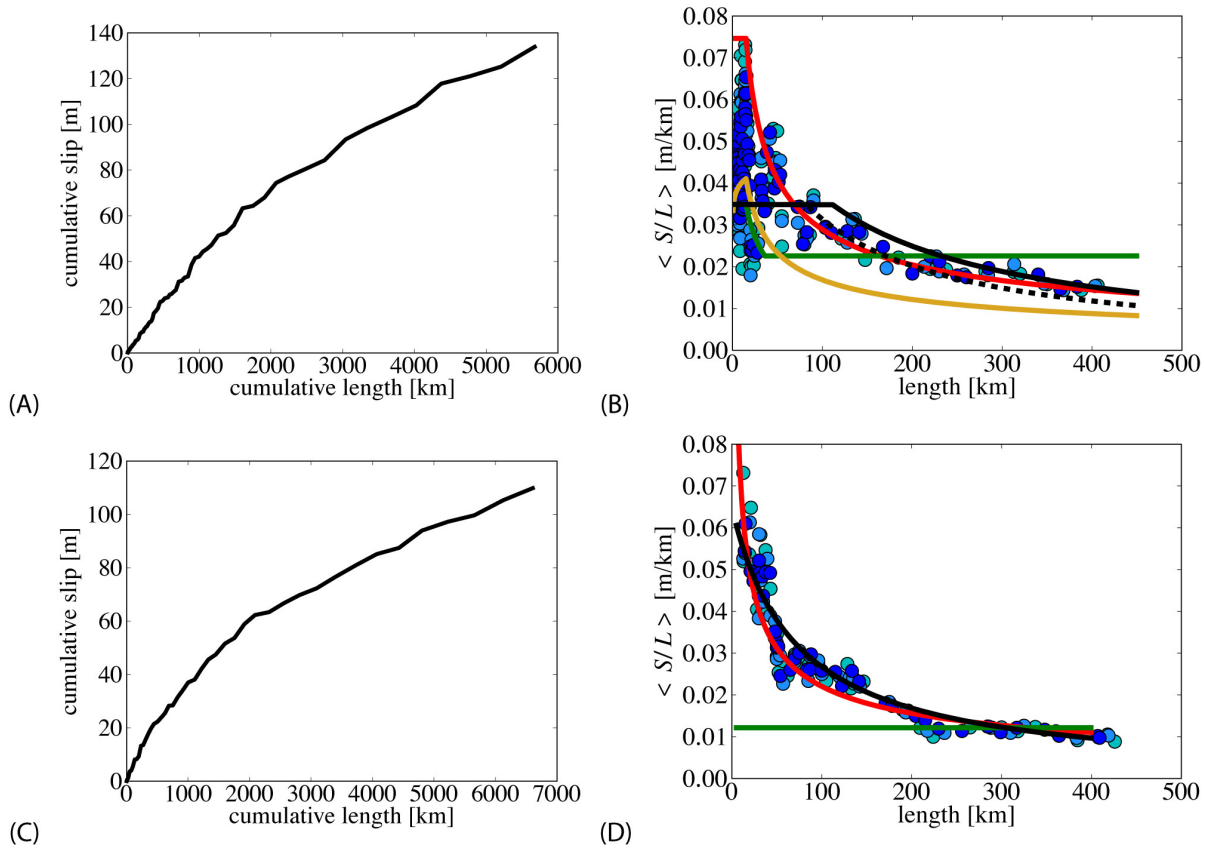

Figure E4. Graphs showing sublinear scaling of slip with length. Top plots use implied slip-length from magnitude-area data. Bottom plots use surface slip-length data. (*A*) Cumulative slip versus cumulative length, showing the sub-linear scaling inherent in the data. Linear scaling implies a straight line on the cumulative curve; downward curvature is sublinear scaling, increasing slower than linear; and upward curvature is supralinear scaling, increasing faster than linear scaling. (*B*) Average slope given by local average slip over average length, plotted as a function of length. The local slope is fit by an average over *n* points in the neighborhood; here *n*=3, 4, 5 in the different colors. The data are implied slip-length from the magnitude-are data of Hanks and Bakun (2008). The different color curves show the different scaling law fits. The curves are the implied slip-length derived from the magnitude area scaling relations: Ellsworth-B, equation 1 (red); Wells-Coppersmith, equation 4 (yellow); Hanks-Bakun, equation 2 (green); and S09, equation 3 (black). The S09′ relation is shown with two default *W* values: 15 km (solid black line), and 11 km (dashed black line). (*C*) Same as (*A*) but instead using surface slip data. (*D*) Same as (*B*) but instead using surface slip data. The different color curves show the different scaling laws fits for the surface slip relations. The data are surface slip-length Biasi and others (appendix F, this report). The curves are $L^{1/2}$, equation 10 (red); *L,* equation 11 (green); and constant stress drop, equation 13 (black).

Other Scaling Relations

Some other scaling relations have been proposed that we did not explicitly examine here. Wesnousky (2008) proposed slip scaling with the log of length. He found the standard deviation for that fit to the data was equivalent to that for an $L^{1/2}$ scaling; given the singularity at 0, the additional parameter required, and the lack of an extension to a corresponding magnitude-area

scaling, we did not consider this a worthwhile functional form to pursue. Various authors have proposed generalized Wells-Coppersmith scaling relations (for example, Yen and Ma, 2011). Leonard (2010) has proposed a set of self-consistent scaling laws based on W scaling with L. In the large L limit, it behaves as $L^{1/2}$; at smaller lengths, it has a different scaling. However, given the scatter in the data and the additional parameters associated with changes at smaller scales, the added complexity and added parameters were considered not worth pursuing here.

It has long been noted that stable continental regions appear to slip about 2–3 times more than plate boundary earthquakes (Kanamori and Anderson, 1975; Scholz, 1994; Leonard, 2010). Further refinement of catalogues to separate out this effect is one question, and some of the large slip earthquakes might be a result of mixing in these types of earthquakes. For the surface slip data, the fact that the California-only regressions were only about 5–10 percent less than the regressions on the global dataset suggest this is not a big effect in the catalogues we used. For the implied slip-length data derived from magnitude-area data, this is likely contributing to some of the differences relative to the surface slip data.

Dipping Faults

The constant-stress-drop model has been generalized for dipping faults and oblique slip (Shaw, 2013). For dip-slip faults, two characteristics affect the scaling. One characteristic is that the downdip width W generally is larger for dipping faults, as discussed later in equation 16. For dips θ of 90° (strike-slip), 60° (normal), and 30° (thrust), the increased width due to dip factor of $1/\sin\theta$ is, respectively, 1, 1.15, and 2. Therefore, this is a significant factor only for shallow dips. A second factor is a change in the coefficient on W for the infinite rupture, with the factor of 2 replaced by $(\lambda + 2\mu)/(\lambda + \mu)=1/(1 - (v_s/v_p)2)$, where v_s/v_p is the ratio of the shear wave speed to the compressional wave speed. Using typical values of v_s/v_p of 1.75 gives typical values about 1.5 for this factor or about three-fourths of the value for dip-slip relative to strike-slip. Therefore, for dip-slip cases, we have

$$S = \frac{\Delta\sigma}{\mu} \frac{1}{\frac{7}{3L} + \frac{1}{(\frac{\lambda+2\mu}{\lambda+\mu})W}} \tag{14}$$

We can further generalize this to the oblique slip case for slip in the arbitrary direction $\hat{\boldsymbol{s}}$ composed of along-strike and dip-slip components:

$$S = \frac{\Delta\sigma}{\mu} \frac{1}{\frac{7}{3L} + \frac{1}{W\hat{s}(2,\frac{\lambda+2\mu}{\lambda+\mu})}} \tag{15}$$

The combined effects for the three dip cases are shown in figure E5, with θ=90° using equation 13, and θ=60° and 30° using equation 14, assuming constant seismogenic depth and correspondingly varying downdip W, and with the later two dip-slip cases including the modulus effect in equation 14.

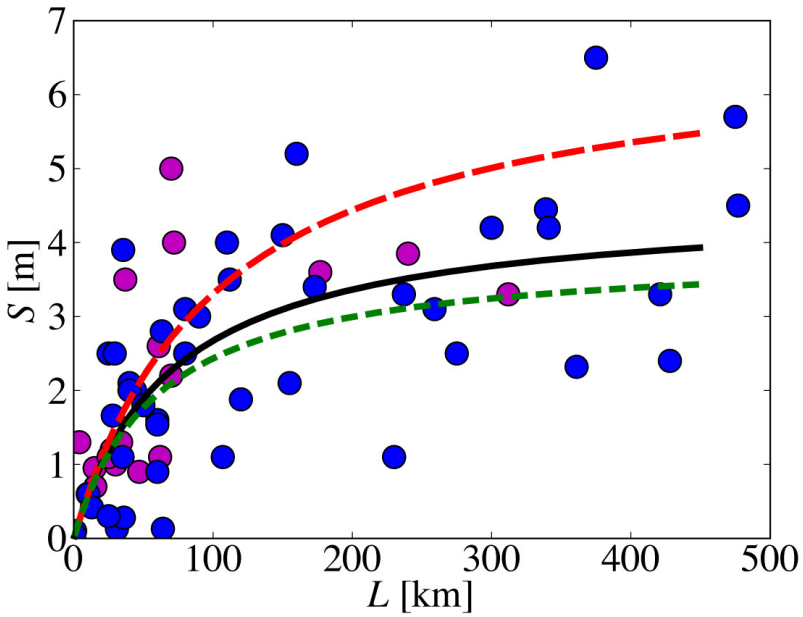

Figure E5. Graph showing dip effects on expected scaling. Data points are geological surface slip observations of average slip versus length from the Biasi and others (appendix F, this report) database. Color indicates focal mechanism: strike-slip shown in blue, dip-slip in magenta. Solid lines show scaling expected for fixed seismogenic depth, but changing dip, and, thus, downdip width and changing modulus effects. All curves have the same stress drop, a value for best fit stress drop to strike-slip data of 4.54 MPa . Different curves use same seismogenic depth of 15 km and different dips 90° (black) strike-slip equation 13, and 60° (green) and 30° (red) dip-slip equation 14. Only relatively small differences are expected in scaling of earthquakes with different focal mechanisms, which appears consistent with data.

We see the modulus effect prevailing over the increased W effect at 60°, so the expected slip is slightly less for the 60°-dip case. The crossover where the two effects are comparable occurs at about 45°. By 30°, the increased W effect dominates and slip increases, but not by a large amount. It is not until there are faults with very shallow dips that a whole new scale of slip appears, at dips and W's relevant to subduction zones. Therefore, for subareal surface rupturing events, under constant-stress-drop scaling we expect similar slips for dip-slip versus strike-slip earthquakes. The data, sparse as it is, appears to support this. The conclusion that dip-slip and strike-slip earthquakes have similar stress drops also has been found in regressions using other types of scaling assumptions (Leonard, 2010). This lends additional support to the approach of treating dip-slip and strike-slip earthquakes similarly.

Branch Recommendations

Four slip-length scaling relations, the two leading implied scalings equations 1 and 3, and the two leading surface scalings equations 10 and 13, are shown in figure E4. The implied slip-length scalings from the magnitude-area scalings are shown with dashed lines, and the slip-length scaling fits to surface slip data are shown in solid lines. The data do not support the linear scaling of slip with length out to the largest lengths. Moreover, given the sensitivity of the exponents in the power-law scaling to the different datasets, and only marginal improvement in

the fitting, opening up to nonspecific exponents is not recommended. We recommend keeping the top two scalings in the two different approaches, which in both the inferred slip-length from magnitude-area and the surface slip-length data show sublinear scaling.

One question regarding the surface slip estimates is whether it is better to use a default W, or to use fault specific values of W. Because the implied slip estimates from the magnitude-area data already use fault-specific values of W, we suggest that a default value of W be used in the surface slip estimates. This approach provides a complementary estimate in the rates that compensates for potential errors in fault-specific W estimates. It sacrifices some potential accuracy for more robustness and more behavior toward the mean. This approach results in errors in rates from surface slip with W that are less correlated with errors in the alternative magnitude-area approach. Given uncertainties in W estimates, and the desirability of spanning the range of estimates, using a default W is a useful complementary approach on this set of branches. Future study could show sufficient added skill in the W estimates to warrant further use of fault-specific W estimates for the rates; however, in the absence of sufficiently demonstrated skill, the uncorrelated approach appears preferable.

Weighting Recommendation for Rates of Events

Sublinear scaling in data disfavors linear η=1 scaling. We see no compelling reason to open up to the continuum, and argue against opening up power law continuum over specific discrete values. There are a number of reasons for this recommendation. We see little if any advantage to using the arbitrary exponent power law fit instead of the two discrete exponent fits; the exponents in the power law change in different datasets. Because exponents are associated with a particular physics, this last feature is especially problematic from a physics-based hazard perspective.

Given the comparability of the fit within the datasets, an equal weighting of the two leading scalings for a given data set is recommended. Given the uncertainty between the branches based on magnitude-area estimates on the one hand, and the branches based on surface slip-length estimates on the other, an equal weighting between the two different types of estimates seems justified. Recommended parameter values are those in tables E2a and E3a. If we wanted to use the California-only dataset (table E3b) rather than the full dataset (table E3a), for consistency, some correction for magnitude-area scaling laws should also be made. Given the small change in best-fitting parameter values (about 5–10 percent), we recommend using the full dataset, table E3a, for the sake of simplicity.

Weighting Recommendation for Sizes and Rates Combined

Looking for consistency in assumptions underlying the scaling laws used for sizes and the scaling laws used for rates is one way to add constraints. This was done implicitly in UCERF2 by using the same scaling laws for the sizes and the earthquakes, and not mixing the two laws used. Using these criteria further discourages the use of the continuum power law solutions because matching power laws on the different datasets would add further nontrivial constraints on physics. It also appears to be sufficiently accounted for in the other sublinear scaling laws. That leaves four clear candidates, if we want compatibility in basic assumptions: (1) equations 1 and 6, (2) equations 1 and 10, (3) equations 3 and 9, and (4) equations 3 and 13. In the case of the Hanks-Bakun, and the associated η=1 linear solution, although it is unfavored by the sublinear scaling in the rate estimate fits, and in fits at large earthquakes, continuity with its use in previous estimates and its role as an outlier justify including it as a potential branch.

Figure E6 illustrates the slip-length scaling relations of the five recommended branches, with three coming from implied slip from magnitude-area scaling, and two coming from surface slip scaling.

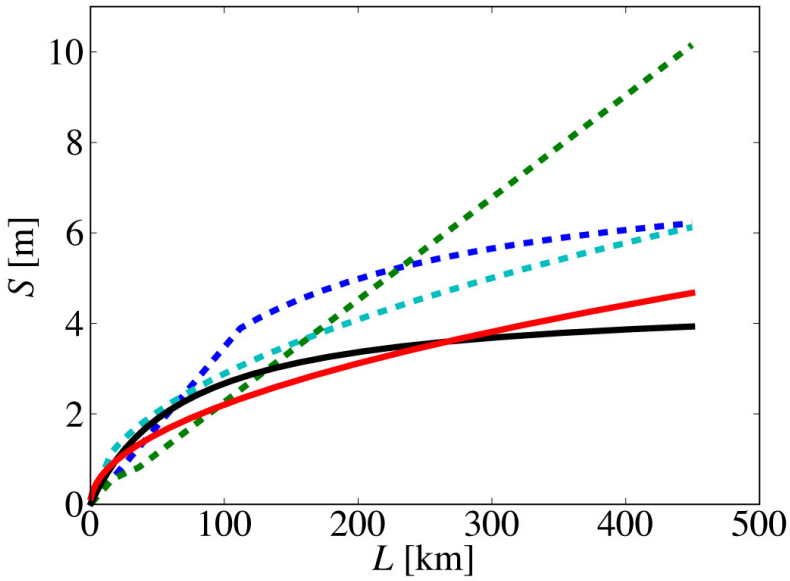

Figure E6. Graph showing slip length scaling relations for large strike-slip events. Dashed lines are implied slip-length scaling relations derived from magnitude-area scaling relations. Solid lines are slip-length scaling relations derived from surface slip observations. The dashed lines are systematically above the solid lines at large lengths. Dashed lines from implied slip-length scaling parameters based on magnitude-area fits, table E2a. Dashed cyan line is implied slip-length from Ellsworth-B (Working Group on California Earthquake Probabilities, 2003) magnitude-area relation, equation 1. Dashed blue line is implied slip-length from S09 equation 3, shown using default W=15 km value. Dashed green line is implied slip-length from Hanks and Bakun (2002) bilinear relation, equation 2. Solid curves are fits to surface slip-length data. Solid red line is $L^{1/2}$ scaling, equation 10. Solid black line is constant stress drop scaling (Shaw, 2013), equation 13. The dashed blue line best fits the slip-length data derived from the magnitude-area data. The solid black line best fits the surface slip-length data.

Logic Tree Recommendation

The recommended combined branches and parameter values are shown in table E4. The full branch sets are shown in table E4a. A potential trimming of the full branch is shown in table E4*B*. An equal weighting of the branches in table E4a is one potential recommended approach with the most branches. A trimming based on consistency between functional forms in sizes and rates, as was done in UCERF2 (shown in table E4b), is an alternative with the fewest branches. An expansion to include previously used branches is shown in table E4c.

Table E4. Logic tree branches.

[Branches in the logic tree are shown in tables 4a–c. (a) Maximal branches showing four viable magnitude-area scaling laws combined with four viable slip-length scaling laws, for a total of 16 branches. (b) Trimmed set of branches using consistency in scaling assumptions, with basis of scaling in sizes consistent with same assumptions underlying scaling in rates. This type of consistency was used in UCERF2. (c) Extension of trimmed consistency set to include previously used branch that also has role as outlier. Default values unless otherwise specified are W=15 km; μ=30 GPa]

(a) Full branches.

Sizes			Rates		
Name	Eqn	Table	Name	Eqn	Table
S09	(3)	E1a	S09	(9)	E2a
			EB	(6)	E2a
			S12	(13)	E3a
			$L^{1/2}$	(10)	E3a
EB	(1)	E1a	S09	(9)	E2a
			EB	(6)	E2a
			S12	(13)	E3a
			$L^{1/2}$	(10)	E3a
HB	(2)	E1a	S09	(9)	E2a
			EB	(6)	E2a
			S12	(13)	E3a
			$L^{1/2}$	(10)	E3a
WC[†]	(4)	E1c	S09	(9)	E2a
			EB	(6)	E2a
			S12	(13)	E3a
			$L^{1/2}$	(10)	E3a

(b) Trimmed by consistency of scaling assumption.

Sizes		Rates	
Name	Eqn	Name	Eqn
S09	(3)	S09	(3)
		S12	(13)
EB	(1)	EB	(1)
		$L^{1/2}$	(10)

(c) Extension of consistency set to previously used branch.

Sizes			Rates		
Name	Eqn	Table	Name	Eqn	Table
S09	(3)	E1a	S09	(3)	E1a
			S12	(13)	E3a
EB	(1)	E1a	EB	(1)	E1a
			$L^{1/2}$	(10)	E3a
HB	(2)	E1a	HB	(2)	E1a

Hazard Sensitivity Tests to Data Uncertainties

Hazard sensitivities to various model components are important to understand. Sensitivity to one data uncertainty could be explored in the following way. A question of whether area estimates of aftershocks may be biased high at the smaller magnitudes (W. Ellsworth, USGS, oral commun. 2009) warrants further observations. Although the data side of this is beyond the scope of what can be accomplished in UCERF3, the hazard sensitivity could be tested. Exploration of the hazard significance of deviations in this range could be studied by exploring a range of parameters in the Shaw09 relations, which has the flexibility to change scaling at small

earthquakes separately from scaling at the largest earthquakes. For example, comparing the hazard from S09′ with (C_0=3.98, W=15 km, β=7.4) against S09′ with a perturbed set of parameters would be a good test of hazard sensitivity to the differences in scaling at small earthquake sizes. Thus, modified parameters ($C_0+\delta C_0$, $W \cdot 10^{\frac{3}{2}\delta C_0}$, $\beta \cdot 10^{-3\delta C_0}$) with, in particular, δC_0=0.22 so as to match the scaling of Ellsworth-B at the small earthquakes, giving modified parameters (C_0=4.20, W=32.0 km, β=1.6), would be an interesting comparison against the unperturbed values. Rates will be affected minimally by any of this because slip sums are dominated by the largest earthquakes.

Depth Extent of Rupture

Relationship between *W* and Seismogenic Depth

Past working groups have used the seismogenic depth H as a proxy for downdip width W during large earthquakes. However, there is some uncertainty as to the precise relationship between W and H. Dynamic ruptures are able to push at least some distance into velocity-strengthening layers, so W may be at least as large as H. Rolandone and others (2004) found a deepening of seismicity following the Landers earthquake. We propose to handle the uncertainty posed by the additional potential deepening with a constant proportionality parameter ξ:

$$W = \xi H / \sin\theta \tag{16}$$

We also have explicitly included in the expression the geometric correction for the fault dip angle θ to transform depth to downdip length. There needs to be a discussion about which values should be used for ξ. We probably can place one bound on ξ because it is unlikely that W would break less deep than H:

$$\xi \geq 1 . \tag{17}$$

In principle, ξ need not be a constant, and could be a function of L, implying that W is a function of L (King and Wesnousky, 2007; Leonard, 2010). This further extension merits additional study. It would, for example, allow the association of the Hanks-Bakun magnitude-area scaling with a sublinear slip-length scaling; one could trade high implied slips instead for high implied downdip widths (though the widths associated with the longest ruptures might be considered problematic). It would, however, lead to additional moment rate estimates for the same slip rates on faults, and because current UCERF3 estimates are already high relative to preferred values, this extension has not yet been examined.

Branch Recommendations

In the tables, we have used Ws of 15 km, a standard value from aftershock data. A value of ξ = 1.25 would be compatible with California observations that H=12 km as well as with Rolandone and others (2004). However, weightings in a logic tree to different values of ξ should be discussed, as this parameter has implications for many different things. ξ =1 and 1.5 are two other values to consider.

Coefficients for the regressions to the California-only data in table E3b also may address questions about which W may be relevant. Here, tectonic differences reflected in stress drops (that is, intraplate versus interplate) and differences in W might tend to increase the global data amplitudes relative to the California-only amplitudes. The fact that California-only amplitudes

differ by only 5–10 percent from the global amplitudes (as reflected in amplitude comparisons of tables E3a and 3b), suggests that global observations should serve as a good guide for what to expect in California.

Faults with Substantial Surface Creep

In locations where surface creep is a substantial fraction of the slip budget, traditional magnitude-area estimates are more appropriate for slip-rate budgeting, and full weighting should be given to those branches of the logic tree. This is a very rare situation for faults. Exceptions in California include the creeping and Parkfield sections of the San Andreas Fault, and the Hayward Fault, but these exceptions prove the rule, constituting a very small fraction of the active faults considered in California hazard calculations (Working Group on California Earthquake Probabilities, 2008). Where there is substantial creep, slip estimates that normally would come from surface slip estimates would instead come from magnitude-area estimates. This is because ruptures where much surface creep is occurring interseismically are expected to have altered rupture areas, and potentially different slip from full seismogenic ruptures represented in the surface slip scaling relations. A simple way to implement the full weighting on the traditional magnitude-area branches is to do this when average aseismicity α averaged along a candidate rupture is above a critical threshold:

$$\langle \alpha \rangle = \frac{1}{L}\int_0^L \alpha(x)dx \geq \alpha_c \qquad (18)$$

with α_c = .2 as a recommended value. Other values of α_c that could be tried include .15 and .3. We only expect minimal effects on hazard estimates from this choice of α_c.

Other Issues Regarding the Depth Extent of Rupture

Variable Width Dip-Slip Faults

Our scaling relations were formulated in terms of a downdip seismogenic width *W*. When this width varies along-strike, the relevant quantity is the average width (to leading order is the arithmetic average *W* that matters in constant stress drop scalings [Shaw, 2009]). With respect to UCERF, which has variable *W's* in its database, there are two ways to handle varying *W*. One way is to take the seismogenic widths as given in the fault database, and to calculate an arithmetic average across candidate length *L* ruptures. This assumes that the variation in the widths in the database are relatively well known beyond only dip information, and that varying seismogenic depth on dipping faults is sufficiently constrained to make the added information useful to incorporate. The second way is to presume the most homogeneous case and to make minimal demands on observations, by assuming a constant seismogenic depth, and to assume all width variations come from dip variations. Both of these ways are straightforward to implement. It would be useful to implement both of them, and to compare the results. Which one would be favored from a branch weight point of view depends on how much confidence there is in deviations of seismogenic depths on dip slip faults relative to default values, and the relationships to downdip rupture.

Physics-Based Ground Motion Simulators

The depth extent of rupture is relevant not only to helping constrain slips and rates in earthquakes, but also as input constraints for statistically based kinematic models of ruptures. Many such models have been developed (for example, Herrero and Bernard, 1994; Mai and Beroz, 2000). Statistically based kinematic models have also been used to forward-model ground motions. In the Cybershake case (Graves and others, 2011), the goal was to get a better estimate of ground motions and hazard in geographically specific settings, replacing ground-motion prediction equations, which relate shaking levels to various rupture parameters such as magnitude and closeness of rupture in generic settings, with geographically specific basin and directivity effects from sets of ruptures for particular velocity models and rupture distributions.

Cybershake (Graves and others, 2011) is outside the scope of UCERF3, but it is, nevertheless, an interested user, and potentially could develop into a useful constraint, feeding back on the scaling laws as a consistency check. We, therefore, focus our attention on Cybershake in this discussion.

Initial efforts Cybershake efforts have encountered difficulties combining magnitude-area scaling laws used in UCERF2 with particular kinematic models to match some features of Ground Motion Prediction Equations (GMPEs). Whether the issues are associated with the scaling laws, the particular kinematic models, the GMPEs, or some combination of these effects is an open question.

Because Cybershake has many underlying assumptions (such as the degree of coherence in the ruptures), sensitivities in Cybershake need to be explored further before it is used as a constraint on UCERF relations. Nevertheless, a goal is to develop compatibility, and, therefore, exploring the implications of the various relations in this context is an important task.

An unresolved epistemic uncertainty in the depth dependence of slip concerns how much coseismic slip may be occurring below the seismogenic layer. Dynamic models suggest a significant fraction of slip may be occurring below the seismogenic layer—as much as about one-third the total moment (Shaw and Wesnousky, 2008). This slip would be occurring mainly as long period motion, with a lack of high frequencies (Shaw and Wesnousky, 2008).

An exponential decay or a linear decay with depth below the seismogenic layer is a reasonable parameterization of what is observed in the dynamic models (Shaw and Wesnousky, 2008). The scale length of the decay depends on the degree of velocity strengthening; the degree of strengthening is not well constrained, and, therefore, the scale length remains an epistemic uncertainty.

The distributions of slip, and rupture velocities, are important factors that warrant further study in Cybershake. Correlations of slip at the surface have Gaussian, or even faster than Gaussian falloff in the tails (Shaw, 2011), so Cybershake simulations with extreme slip values in the distributions (for example, 50 meters slip in great strike-slip earthquake patches) should be reexamined. Recent lidar measurements of surface offsets in California confirm this lack of high slip values.

Given the implied high stress drops at moderate earthquake magnitudes in the Ellsworth-B relations, and the implied high stress drops at large earthquake magnitudes in the Hanks-Bakun relations, it would be interesting to study whether constant stress drop models are compatible with Cybershake. For example, is the Shaw09 magnitude-area scaling relation, combined with a 30-percent subseismogenic high-frequency deficient moment, compatible with higher variance rupture velocity, low variance slip patch versions of Cybershake?

References Cited

Akaike, H., 1974, A new look at the statistical model identification: Institute of Electrical and Electronics Engineers Transactions on Automatic Control, v. 19, no. 6, p. 716–723.

Das, S., 1982, Appropriate boundary conditions for modeling very long earthquakes and physical consequences, 1982: Bulletin of the Seismological Society of America, v. 72, no. 6A, p. 1911–1926.

Graves, R., Jordan, T,H., Callaghan, S., Deelman, E., Field, E., Juve, G., Kesselman, C., Maechling, ., Mehta, G., Milner, K., Okaya, D., Small, P., and Vahi, K., 2011, Cybershake—A physics-based seismic hazard model for Southern California: Pure and Applied Geophysics, v. 168, nos. 3–4, p. 367–381.

Hanks, T.C., and Bakun, W.H., 2002, A bilinear source-scaling model for M-log A observations of continental earthquakes: Bulletin of the Seismological Society of America, 2002, v. 92, no. 5, p. 1841–1846.

Hanks, T.C., and Bakun, W.H., 2008, M-log A observations of recent large earthquakes: Bulletin of the Seismological Society of America, v. 98, no. 1, p. 490–494.

Herrero, A., and Bernard, P., 1994, A kinematic self-similar rupture process for earthquakes: Bulletin of the Seismological Society of America, v. 84, no. 4, p. 1216–1228.

Kanamori, H., and Anderson, D. L., 1975, Theoretical basis for some empirical relations in seismology: Bulletin of the Seismological Society of America, V. 65, no. 5, p. 1073–1095.

King, G. L., and Wesnousky, S., 2007, Scaling of fault parameters for continental strike-slip earthquakes: Bulletin of the Seismological Society of America, v. 97, no. 6, p. 1833–1840.

Knopoff, L., 1958, Energy release in earthquakes: Geophysical Journal of the Royal Astronomical Society, v., 1, no. 1, p. 44–52.

Leonard, M., 2010, Earthquake fault scaling—Self-consistent relating of rupture length, width, average displacement, and moment release: Bulletin of the Seismological Society of America, v. 100, no. 5A, p. 1971–1988.

Mai, P.M., and Beroza, G.C., 2000, Source scaling properties from finite–fault-rupture models: Bulletin of the Seismological Society of America, v. 90, no. 3, p. 604–615.

Rolandone, F., Bürgmann, R., and Nadeau, R.M., 2004, The evolution of the seismic-aseismic transition during the earthquake cycle—Constraints from the time-dependent depth distribution of aftershocks: Geophysical Research Letters, v. 31, L23610, doi:10.1029/2004GL021379 .

Romanowicz, B., 1992, Strike-slip earthquakes on quasi-vertical transcurrent fault—Inferences for general scaling relations: Geophysical Research Letters, v. 19, no. 5, p. 481–484.

Scholz, C.H., 1994, Reply to comments on “A reappraisal of large earthquake scaling” by C. Scholz: Bulletin of the Seismological Society of America, v. 84, no. 5, p. 1677–1678.

Shaw, B.E., 2009, Constant stress drop from small to great earthquakes in magnitude-area scaling: Bulletin of the Seismological Society of America, v. 99, no. 2A, p. 871–875.

Shaw, B.E., 2011, Surface slip gradients of large earthquakes: Bulletin of the Seismological Society of America, v. 101, no. 2, p. 792–804.

Shaw, B.E., 2013, Earthquake surface slip-length data is fit by constant stress drop and is useful for seismic hazard analysis: Bulletin of the Seismological Society of America, v, 103, no. 2A, p. 876–893.

Shaw, B.E., and Wesnousky, S.G., 2008, Slip-length scaling in large earthquakes: The role of deep-penetrating slip below the seismogenic layer: Bulletin of the Seismological Society of America, v. 98, no. 4, p. 1633–1641.

Somerville, P.G., 2006, Review of magnitude-area scaling of crustal earthquakes: Report to Working Group on California Earthquake Prediction: Pasadena, Calif., URS Corporation, 22p.

Starr, A.T., 1928, Slip in a crystal and rupture in a solid due to shear: Mathematical Proceedings of the Cambridge Philosophical Society, v. 24, no. 4,, p. 489–500.

Wells, D.L., and Coppersmith, K.J., 1994, New empirical relationships among magnitude, rupture length, rupture width, rupture area, and surface displacement: Bulletin of the Seismological Society of America, v. 84, no. 4, p. 974–1002.

Wesnousky, S.G., 2008, Displacement and geometrical characteristics of earthquake surface ruptures—Issues and implications for seismic-hazard analysis and the process of earthquake rupture: Bulletin of the Seismological Society of America, v. 98, no.4, p. 1609–1632.

Working Group on California Earthquake Probabilities, 2003, Earthquake probabilities in the San Francisco Bay Region—2002 to 2031: U.S. Geological Survey Open-File Report 2003–214, *http://pubs.usgs.gov/of/2003/of03-214/.*

Working Group on California Earthquake Probabilities, 2008, The Uniform California Earthquake Rupture Forecast, version 2 (UCERF2): U.S. Geological Survey Open-File Report 2007-1437, 96 p.

Yen, Y.T., and Ma, K.F., 2011, Source-scaling relationship for M 4.6–8.9 earthquakes, specifically for earthquakes in the collision zone of Taiwan: Bulletin of the Seismological Society of America, v. 101, no. 2, p. 468–481.